

# Thermoelectric properties of finite two dimensional triangular lattices coupled to electrodes

David M T Kuo

*Department of Electrical Engineering and Department of Physics,  
National Central University, Chungli, 320 Taiwan*

(Dated: September 25, 2020)

Novel intrinsic two-dimensional materials have attracted many researchers' attention. The unusual transport and optical properties of these materials originate mainly from triangular lattices (TLs). Therefore, the application of energy harvesting calls for a study of the thermoelectric properties of 2D TLs coupled to electrodes. The transmission coefficient of 2D TLs is calculated by using the Green's function technique to treat ballistic transports. Especially important among our findings is the electron-hole asymmetric behavior of the power factor ( $PF$ ). Specifically, the maximum  $PF$  of electrons is significantly larger than that of holes. At room temperature, the maximum  $PF$  of electrons is dictated by the position of the chemical potential of electrodes near the band edge of TLs. The enhancement of  $PF$  with increasing electronic states results from the enhancement of electrical conductance and constant Seebeck coefficient. When the band gap is ten times larger than the thermal energy, it is appropriate to make one-band model predictions for thermoelectric optimization.

## I. INTRODUCTION

Designing a thermoelectric material with a high figure of merit ( $ZT$ ) and optimized power output has been under intensive pursuit in energy harvesting applications [1-4]. The dimensionless figure of merit  $ZT = S^2 G_e T / \kappa$  depend on the Seebeck coefficient ( $S$ ), electrical conductance ( $G_e$ ) and thermal conductance ( $\kappa$ ) of the material. Thermoelectric materials with a delta-function transmission coefficient show impressive  $ZT$  values [1]. This inspires one to study the thermoelectric properties of individual quantum dot (QD) systems [2,5-7]. However, such QD systems yield low electrical power outputs. Another approach to increasing  $ZT$  is to reduce the thermal conductance of thermoelectric materials [3],[8]-10]. Although the  $ZT$  value of 3D QD superlattices can reach a remarkable value of two [10], it is difficult to raise it to larger than three. Two dimensional systems offer high potential to achieve  $ZT > 3$  due to their reduced phonon thermal conductance ( $\kappa_{ph}$ ). [3] If a material is found with  $ZT \geq 3$ , thermoelectric refrigerators will become competitive against conventional compressor-based systems [12]. Moreover, QD superlattice systems suffer from the problem of size and position fluctuation, which seriously reduces the  $G_e$  and  $ZT$  of QD arrays [11]. Solving these problems is critical for the applications of thermoelectric devices consisting of QD solid crystals [12].

Intrinsic two-dimensional materials (ITDMs) such as 2D transition metal dichalcogenides (TMDCs) and oxides (TMOs) have attracted much attention due to their stable structures and widely tunable electronic band structures by using external forces such as electric field and strain [13-15]. In addition, the thermal conductivity of ITDMs is much smaller than that of their corresponding bulk materials [16-18]. Although the thermoelectric properties of ITDMs have been theoretically studied using the first-principle method [19-23], the contact and size effects on the electron transport of their heterostruc-

tures are still unclear [24]. Because the unusual transport and optical properties of ITDMs originate mainly from the triangular (hexagonal) lattices (TLs) [25-28], their potential application to micro power generators and refrigerators calls for an investigation of the thermoelectric properties of finite 2D TLs coupled to electrodes as shown in Fig. 1. A finite 2D TMDC also plays an important role in building quantum registers and nanoscale transistors [29-32]. This study has several important findings: (a) the power factor ( $PF$ ) shows an electron-hole asymmetric behavior, (b) the maximum  $PF$  of the electrons is significantly larger than that of the holes, and (c) the maximum  $PF$  of electrons at room temperature occurs at the position of the chemical potential of electrodes near the band edge of TLs. Moreover, we also reveal the contact, size, and geometry effects on the thermoelectric properties of TLs in the ballistic transport process. These conclusions are meaningful insights for further improvement of the performance of micro thermoelectric devices consisting of intrinsic 2D materials.

## II. FORMALISM

To model the thermoelectric properties of a finite 2D TL connected to the electrodes, the Hamiltonian of the system shown in Fig. 1 is given by  $H = H_0 + H_{QD}$ , [33] where

$$H_0 = \sum_{k,\sigma} \epsilon_k a_{k,\sigma}^\dagger a_{k,\sigma} + \sum_{k,\sigma} \epsilon_k b_{k,\sigma}^\dagger b_{k,\sigma} \quad (1)$$

$$+ \sum_{\ell} \sum_{k,\sigma} V_{k,\ell,j}^L d_{\ell,j,\sigma}^\dagger a_{k,\sigma} + \sum_{\ell} \sum_{k,\sigma} V_{k,\ell,j}^R d_{\ell,j,\sigma}^\dagger b_{k,\sigma} + H.c.$$

The first two terms of Eq. (1) describe the free electron gas in the left and right electrodes.  $a_{k,\sigma}^\dagger$  ( $b_{k,\sigma}^\dagger$ ) creates an electron of momentum  $k$  and spin  $\sigma$  with energy  $\epsilon_k$  in the left (right) electrode.  $V_{k,\ell,j}^L$  ( $V_{k,\ell,j}^R$ ) describes the

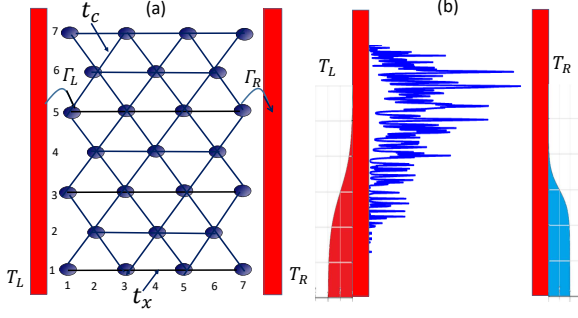


FIG. 1: (a) Schematic diagram of finite two dimensional triangular lattices (2D TLs) coupled to electrodes.  $\Gamma_L$  ( $\Gamma_R$ ) denotes the tunneling rate of the electrons between the left (right) electrode and the leftmost (rightmost) lattices.  $t_x$  and  $t_c$  are the nearest neighbor hopping parameters along the x and  $\pm\pi/3$ , respectively. (b) Transmission spectra of finite TLs coupled to electrodes with different equilibrium temperatures ( $T_L$  and  $T_R$ ).

coupling between the left (right) lead with its adjacent lattice in the  $\ell$ th row, which counts only for odd rows.

$$H_{QD} = \sum_{\ell,j,\sigma} E_{\ell,j} d_{\ell,j,\sigma}^\dagger d_{\ell,j,\sigma} \quad (2)$$

$$+ \sum_{\sigma} \sum_{\ell_1, \ell_2} \sum_{j_1, j_2}^{N_y} t_{\ell_1, \ell_2, j_1, j_2} d_{\ell_1, j_1, \sigma}^\dagger d_{\ell_2, j_2, \sigma} + H.c.,$$

$$t_{\ell_1, \ell_2, j_1, j_2} = \begin{cases} -t_c & \text{if } |\ell_1 - \ell_2| = 1, |j_1 - j_2| = 1 \\ -t_x & \text{if } |\ell_1 - \ell_2| = 0, |j_1 - j_2| = 2 \end{cases} \quad (3)$$

where  $E_{\ell,j}$  is the atomic energy level of lattice in the TLs. For simplicity, we have considered one orbit for each atom. The spin-independent  $t_{\ell_1, \ell_2, j_1, j_2}$  describes the electron hopping strength between the lattices, which follows the regulation of Eq. (3).  $d_{\ell_1, j_1, \sigma}^\dagger$  ( $d_{\ell_2, j_2, \sigma}$ ) creates (destroys) one electron in the lattice at the  $\ell$ th row and  $j$ th column.

To study the transport properties of a finite TL junction connected to electrodes, it is convenient to use the Keldysh-Green's function technique[33]. Electron and heat currents leaving electrodes can be expressed as

$$J = \frac{2e}{h} \int d\varepsilon T_{LR}(\varepsilon) [f_L(\varepsilon) - f_R(\varepsilon)], \quad (4)$$

and

$$Q_{e,L(R)} = \frac{\pm 2}{h} \int d\varepsilon T_{LR}(\varepsilon) (\varepsilon - \mu_{L(R)}) [f_L(\varepsilon) - f_R(\varepsilon)] \quad (5)$$

where  $f_\alpha(\varepsilon) = 1/\{\exp[(\varepsilon - \mu_\alpha)/k_B T_\alpha] + 1\}$  denotes the Fermi distribution function for the  $\alpha$ -th electrode, where  $\mu_\alpha$  and  $T_\alpha$  are the chemical potential and the temperature of the  $\alpha$  electrode.  $e$ ,  $h$ , and  $k_B$  denote the

electron charge, the Planck's constant, and the Boltzmann constant, in that order.  $T_{LR}(\varepsilon)$  denotes the transmission coefficient of a finite TL connected to electrodes, which can be solved by the formula  $T_{LR}(\varepsilon) = 4Tr[\hat{\Gamma}_L \hat{G}_{D,A}^r(\varepsilon) \hat{\Gamma}_R \hat{G}_{D,A}^a(\varepsilon)]$ , where the matrix of tunneling rates ( $\hat{\Gamma}_L$  and  $\hat{\Gamma}_R$ ) and Green's functions ( $\hat{G}_{D,A}^r(\varepsilon)$  and  $\hat{G}_{D,A}^a(\varepsilon)$ ) are constructed by fortran coding. Note that tunneling rates ( $\Gamma_{L(R), \ell, j}(\varepsilon) = 2\pi \sum_k |V_{k, \ell, j}^{L(R)}|^2 \delta(\varepsilon - \varepsilon_k) = \Gamma_{t, \ell, j}$ ) are assumed as energy-independent physical parameters for simplicity's sake.[34]

The electrical conductance ( $G_e$ ), Seebeck coefficient ( $S$ ) and electron thermal conductance ( $\kappa_e$ ) can be evaluated by using Eqs. (4) and (5) with a small applied bias  $\Delta V = (\mu_L - \mu_R)/e$  and cross-junction temperature difference  $\Delta T = T_L - T_R$ . We arrived at these thermoelectric coefficients:  $G_e = e^2 \mathcal{L}_0$ ,  $S = -\mathcal{L}_1/(eT \mathcal{L}_0)$  and  $\kappa_e = \frac{1}{T}(\mathcal{L}_2 - \mathcal{L}_1^2/\mathcal{L}_0)$ .  $\mathcal{L}_n$  is given by

$$\mathcal{L}_n = \frac{2}{h} \int d\varepsilon T_{LR}(\varepsilon) (\varepsilon - \mu)^n \left(-\frac{\partial f(\varepsilon)}{\partial \varepsilon}\right), \quad (6)$$

where  $f(\varepsilon) = 1/(\exp^{(\varepsilon - \mu)/k_B T} + 1)$  is the Fermi distribution function of electrodes at equilibrium temperature  $T$  and chemical potential  $\mu$ .

### III. RESULTS AND DISCUSSION

Although the density of states (DOS) of triangular lattices has been studied since very early on, there is hardly any literature about the calculation of transmission coefficients of a small-scale 2D TL [35]. Using the Green's function techniques, we calculate  $T_{LR}(\varepsilon)$  in Fig. 2 as functions of  $\varepsilon$  for three configurations (different sets of  $t_x$  and  $t_c$ ) at  $\Gamma_{L(R), \ell, j} = \Gamma_t = 1\Gamma_0$  and  $N_x = N_y = N = 19$ . The inhomogenous spectra of  $T_{LR}(\varepsilon)$  show not only the distribution of electronic states but also the probability of the electrons in the electrodes tunneling through these states. The density of electronic states for a negative regime ( $\varepsilon - E_0 < 0$ ) is higher than that of a positive regime ( $\varepsilon - E_0 > 0$ ). This is consistent with the DOS of TL.[35] The distribution range of electronic states can be explained by an anisotropic electron dispersion relation  $E(\varepsilon) = E_0 - 2t_x(\cos(k_x) + 2\gamma \cos(k_x/2)\cos(\sqrt{3}k_y/2))$ , where  $\gamma = t_c/t_x$  and  $E_0$  denotes the atomic energy level.  $k_x$  and  $k_y$  are dimensionless wave numbers, which depend on  $N_x$  and  $N_y$ . The lower band edge (LBE) and upper band edge (UBE) are, respectively,  $-2t_x(1 + \gamma^2/2)$  and  $2t_x(1 + 2\gamma)$  when  $\gamma = t_c/t_x \leq 2$ . LBE is replaced by  $-2t_x(2\gamma - 1)$  as  $\gamma > 2$ . For example, we have  $LBE = -36\Gamma_0$ ,  $UBE = 72\Gamma_0$  and band width  $BW = 108\Gamma_0$  in Fig. 2(a). All physical parameters are in units of  $\Gamma_0$ . According to Ref.[1], highly efficient thermoelectric materials prefer  $T_{LR}(\varepsilon)$  with a delta function distribution (or  $\frac{BW}{k_B T} \leq 1$ ). This study will focus on the situation of  $\frac{BW}{k_B T} \gg 1$ , because this is an essential condition of TMDC materials at room temperature.

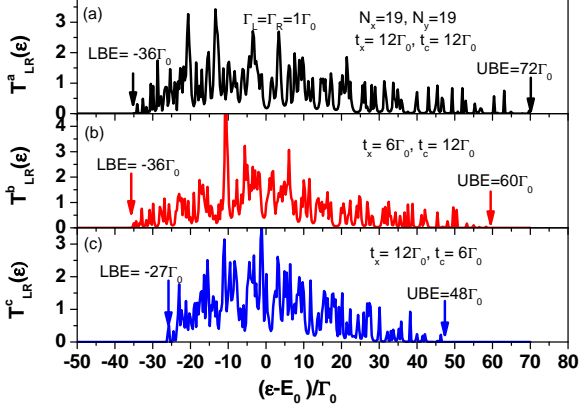


FIG. 2: Transmission coefficient  $T_{LR}(\varepsilon)$  as functions of  $\varepsilon$  for different sets of  $t_x$  and  $t_c$  at  $\Gamma_{L(R),\ell,j} = \Gamma_t = 1 \Gamma_0$  and  $N_x = N_y = N = 19$ . Diagrams (a), (b) and (c) correspond, respectively, to configurations described by  $t_x = 12\Gamma_0$  ( $t_c = 12\Gamma_0$ ),  $t_x = 6\Gamma_0$  ( $t_c = 12\Gamma_0$ ), and  $t_x = 12\Gamma_0$  ( $t_c = 6\Gamma_0$ ). We set  $E_0 = 0$  throughout this article.

Next, we examine the thermoelectric properties of TLs with the three aforementioned configurations. In Fig. 3 we calculate  $G_e$ ,  $S$  and power factor ( $PF = S^2 G_e$ ) as functions of chemical potential ( $\mu$ ) for different  $T_{LR}(\varepsilon)$  configurations at  $k_B T = 2.5\Gamma_0$  and  $k_B T = 5\Gamma_0$ , respectively. Each curve of  $G_e$  at a finite temperature has two components resulting from the resonant tunneling procedure (RTP) and thermionic-assisted tunneling procedure (TATP), respectively (see Fig. 6(d)). When the position of  $\mu$  is within the band regime, RTP (TATP) dominates the electron transport between the electrodes at low (high) temperatures. On the other hand, TATP fully dominates the electron transport, when the position of  $\mu$  is outside the band regime. In Fig. 3(b) and 3(e), Seebeck coefficient is highly suppressed in the conducting regime, while significant  $S$  values appear in the insulating regime. We introduce the picture of hole-transport to describe a positive Seebeck coefficient. Holes are the empty electronic states below  $\mu$ . The maximum  $PF$  is given by the configuration shown in Fig. 2(c) and there exists an asymmetrical electron-hole power factor, as seen in Fig. 3(c) and 3(f). Since  $PF_{max,e}$  is larger than  $PF_{max,h}$ ,  $PF$  prefers the electronic states of TLs above the chemical potential. We note that the positions of  $\mu$  corresponding to  $PF_{max,e}$  values are different at different temperatures. They are  $\mu = -26\Gamma_0$  and  $\mu = -28\Gamma_0$  for  $k_B T = 2.5\Gamma_0$  and  $k_B T = 5\Gamma_0$ , respectively. The position of the chemical potential appears at the left side of LBE for  $k_B T = 5\Gamma_0$ . This indicates that  $PF_{max,e}$  prefers  $\mu$  far away from the band center  $E_0$  at high temperatures. Although electron hopping strengths of TLs can be changed by electric fields[13-15], we will only focus on  $t_x = t_c$  configuration in the following discussion.

To clarify the contact effect between the electrodes and the TLs, we have calculated  $T_{LR}(\varepsilon)$  for different tunnel-

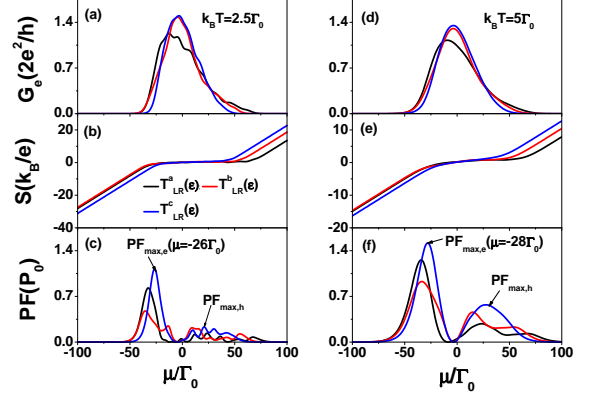


FIG. 3: (a) Electrical conductance  $G_e$ , (b) Seebeck coefficient  $S$  and (c) power factor  $PF$  as functions of  $\mu$  for different configurations shown in Fig. 2 at  $k_B T = 2.5\Gamma_0$ .  $P_0 = \frac{2k_B^2}{h}$ . The curves of (d), (e) and (f) are calculated at  $k_B T = 5\Gamma_0$ . Other physical parameters are the same as those of Fig. 2. The units of  $k_B/e$  and  $P_0$  are  $86.25\mu V/K$  and  $0.58pW/K^2$ , respectively.

ing rate values ( $\Gamma_t$ ) at  $t_x = t_c = 6\Gamma_0$  in Fig. 4(a).  $T_{LR}(\varepsilon)$  is distributed between  $LBE = -18\Gamma_0$  and  $UBE = 36\Gamma_0$ . A large enhancement of  $T_{LR}(\varepsilon)$  is observed as  $\Gamma_t$  increases. Nevertheless, such an enhancement exists only for positive  $\varepsilon$  when we further increases tunneling rate up to  $\Gamma_t = 12\Gamma_0$ . To examine contact effect on thermoelectric coefficients, we have calculated  $G_e$ ,  $S$  and  $PF$  in Fig. 4(b)-4(d) as functions of  $\mu$  at  $k_B T = 2.5\Gamma_0$ . The maximum  $G_e$  occurs at  $\mu = -5, -1$  and  $2\Gamma_0$  for  $\Gamma_t = 1, 6$  and  $12\Gamma_0$ , respectively.  $S$  is vanishingly small when  $G_e$  reaches a maximum value. Unlike  $G_e$ ,  $S$  is not sensitive to the variation of  $\Gamma_t$ . As a consequence, the trend of power factor with respect to  $\Gamma_t$  is same as the trend of  $G_e$ . However,  $PF_{max,e}$  occurs at  $\Gamma_t = 6\Gamma_0$  but not  $\Gamma_t = 12\Gamma_0$ . On the other hand,  $PF_{max,h}$  occurs at  $\Gamma_t = 12\Gamma_0$ . It is worth noting that  $PF_{max,e}$  ( $PF_{max,h}$ ) is given by  $\mu = -16\Gamma_0$  ( $\mu = 33\Gamma_0$ ), which approaches the LBE (UBE). The results in Fig. 4 show that the optimization of PF largely depends on the contact properties.

To reveal the size effect of TLs, we have calculated  $G_e$ ,  $S$ , and  $PF$  in Fig. 5 as functions of  $\mu$  for different  $N$  values at  $k_B T = 2.5\Gamma_0$ . As seen in Fig. 5(a),  $G_e$  increases with increasing  $N$ . It is attributed to the increasing area of  $T_{LR}(\varepsilon)$ . The enhancement of  $G_e$  will unavoidably suppress  $S$  because  $S$  is related to  $G_e$ . Nevertheless, we see that the enhancement of  $G_e$  with increasing electronic states does not suppress  $S$  in Fig. 5(b). As a consequence, we observe the enhancement of  $PF$  with increasing  $N$  in Fig. 5(c). A remarkable thermoelectric device needs a high efficiency and significant power output. Now we discuss the dimensionless figure of merit  $ZT$ , which is given by

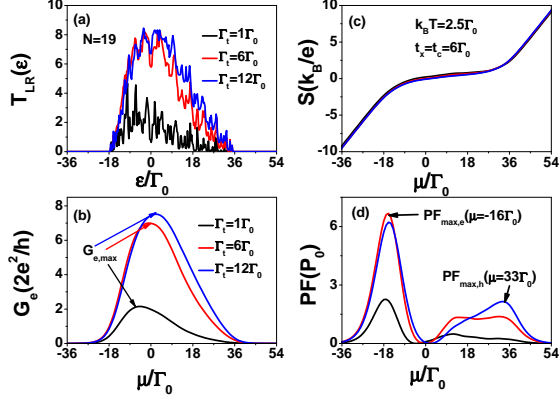


FIG. 4: (a) Transmission coefficient as functions of  $\epsilon$  for various tunneling rates at  $t_x = t_c = 6 \Gamma_0$  and  $N = 19$ . (b) Electrical conductance  $G_e$ , (c) Seebeck coefficient  $S$  and (d) power factor  $PF$  as functions of  $\mu$  for different tunneling rates ( $\Gamma_t$ ) at  $k_B T = 2.5 \Gamma_0$ ,  $t_x = t_c = 6 \Gamma_0$  and  $N = 19$ .

$$ZT = \frac{S^2 G_e T}{\kappa_e + \kappa_{ph}} \quad (7)$$

$$= \frac{\Lambda}{1 - \Lambda + A},$$

where  $\Lambda = \mathcal{L}_1^2 / (\mathcal{L}_1 \mathcal{L}_2)$ , and  $A = \frac{T \kappa_{ph}}{\mathcal{L}^2}$ .  $\kappa_{ph}$  is phonon thermal conductance. One can find that the largest value of  $ZT$  is given by  $\Lambda \rightarrow 1$  and  $A \rightarrow 0$ . Fig. 5(d) shows the maximum  $ZT_{max} = S^2 / L_0$  value as functions of  $\mu$  at  $k_B T = 2.5 \Gamma_0$  in the case of  $\kappa_{ph} = 0$  ( $A = 0$ ).  $L_0 = \kappa_e / (T G_e)$  is the Lorenz number. The maximum  $ZT$  values are  $ZT_{LBE} = 3.3$  and  $ZT_{UBE} = 2.9$  for the positions of  $\mu$  at LBE and UBE, respectively. We note that  $ZT_{LBE}$  is greater than three. Although  $(ZT)_{max}$  shows a significant value when  $\mu$  is far away from the LBE, its  $PF$  becomes vanishingly small. When compared with the band structures of TMDC and TMO materials calculated by the first-principle method,[19-23] we estimate  $\Gamma_0$  to be between  $5 \text{ meV}$  and  $15 \text{ meV}$ . In this work, we adopt  $\Gamma_0 = 10 \text{ meV}$ . The maximum  $PF$  of electrons (holes) at room temperature ( $k_B T = 25 \text{ meV}$ ) occurs at near the LBE (UBE).

In the previous results, we have focused on a TL with  $N_x = N_y$  condition. Fig. 6 shows the calculated  $G_e$ ,  $S$  and  $PF$  as functions of  $\mu$  for different  $N_y$  values at  $k_B T = 2.5 \Gamma_0$  and  $N_x = 51$ .  $G_e$  increases with increasing  $N_y$ . Nevertheless,  $G_e$  does not change if one increases  $N_x$  ( $N_x > 51$ ) at a fixed  $N_y$  value (not shown here). This implies that the enhancement of  $G_e$  with increasing electronic states is attributed to increasing the contact area between the electrodes and the TL. As shown in Fig. 6(b),  $S$  does not change when  $G_e$  increases with increasing electronic states. As seen in Fig. 6(c), the maximum  $PF$  of electrons occurs near LBE even though

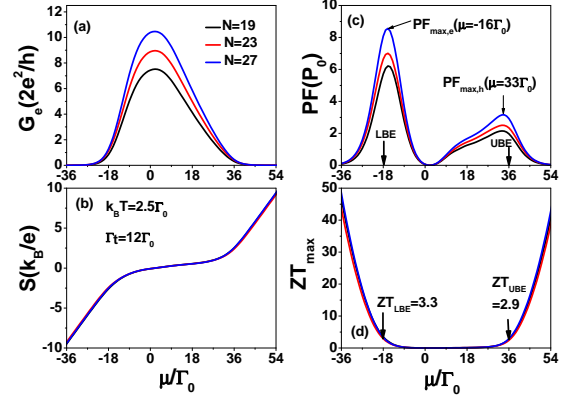


FIG. 5: (a) Electrical conductance, (b) Seebeck coefficient, (c) power factor and (d) figure of merit ( $ZT$ ) as functions of  $\mu$  for various  $N$  values at  $\Gamma_t = 12 \Gamma_0$  and  $k_B T = 2.5 \Gamma_0$ . Other physical parameters are the same as those of Fig.4.

the TL shows a nanoribbon pattern. Because the energy harvesting of thermoelectric devices is expected to operate in a wide temperature range, we calculate  $G_e$ ,  $S$  and  $PF$  as functions of temperature for different  $\mu$  values at  $N_y = 7$  and  $N_x = 51$  in diagrams (d), (e) and (f), in that order. For  $\mu = -16 \Gamma_0$ , a finite  $G_e$  is mainly contributed from RTP at low temperatures. When  $\mu = -20 \Gamma_0$ , the electron transport is dominated by the TATP. As a result,  $G_e$  is numerically significant only at high temperatures.  $S$  is very sensitive to  $\mu$  as  $T \rightarrow 0$ . The curve of  $\mu = -16 \Gamma_0$  shows the best  $PF$  in a wide temperature range ( $k_B T \leq 5 \Gamma_0$ ), as seen in Fig. 6(d).

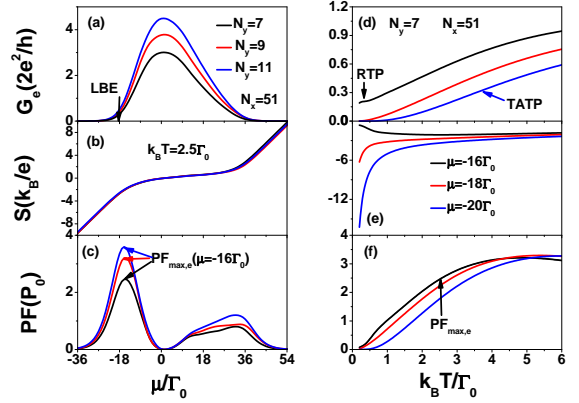


FIG. 6: (a) Electrical conductance  $G_e$ , (b) Seebeck coefficient  $S$ , and (c) power factor  $PF$  as functions of  $\mu$  for various  $N_y$  values at  $N_x = 51$  and  $k_B T = 2.5 \Gamma_0$ . Other physical parameters are the same as those of Fig. 5. (d), (e) and (f) are, respectively,  $G_e$ ,  $S$  and  $PF$  as functions of temperature for different  $\mu$  values at  $N_y = 7$  and  $N_x = 51$ .

So far, our discussions are restricted to the one-band model. The proximity effect between the bands that in-

fluences the thermoelectric properties of ITDMs should also be clarified. To address this problem, we consider that each band has homogenous electronic states and that  $T_{LR}(\varepsilon)$  is given by

$$T_{LR}(\varepsilon) = \begin{cases} A_c & \text{if } E_{CBM} + \Delta_c \geq \varepsilon \geq E_{CBM}, \\ A_v & \text{if } E_{VBM} \geq \varepsilon \geq E_{VBM} + \Delta_v, \\ 0 & \text{otherwise} \end{cases} \quad (8)$$

$E_{CBM}$  and  $E_{VBM}$  denote the conduction band minimum and valence band maximum, respectively. Their band widths are  $\Delta_c$  and  $\Delta_v$ . Band gap is defined as  $E_g = E_{CBM} + |E_{VBM}|$ . Although Eq. (8) is too simple to describe the phenomena resulting from the variances in size, electron hopping strength, contact, and geometry, we can obtain a closed-form solution of the Seebeck coefficient. The analytical forms of  $G_e = G_{e,c} + G_{e,v}$  and  $S = (S_c + S_v)/G_e$  are

$$G_{e,c} = -\frac{e^2 A_c}{2h} (\tanh(y_1) - \tanh(y_2)), \quad (9)$$

$$G_{e,v} = -\frac{e^2 A_v}{2h} (\tanh(z_1) - \tanh(z_2)), \quad (10)$$

$$S_c = \frac{ek_B A_c}{h} [(y_1 \tanh(y_1) - \log(\cosh(y_1))) - (y_2 \tanh(y_2) - \log(\cosh(y_2)))] \quad (11)$$

and

$$S_v = \frac{ek_B A_v}{h} [(z_1 \tanh(z_1) - \log(\cosh(z_1))) - (z_2 \tanh(z_2) - \log(\cosh(z_2)))] \quad (12)$$

with variables  $y_1 = \frac{E_{CBM} - \mu}{2k_B T}$ ,  $y_2 = \frac{E_{CBM} + \Delta_c - \mu}{2k_B T}$ ,  $z_1 = \frac{E_{VBM} + \Delta_v - \mu}{2k_B T}$ , and  $z_2 = \frac{E_{VBM} - \mu}{2k_B T}$ . Using Eqs. (9)-(12), we have calculated  $S$  and  $PF$  as functions of  $\mu$  for two different temperatures in Fig. 7. To reveal the proximity effect, two curves considering one-band model ( $A_v = 0$ ) are also plotted. The second band dramatically changes the behavior of  $S$ , which is vanishingly small near the center of the band gap. The proximity effect can be ignored if the ratio of  $E_g/(2k_B T)$  is greater than ten. This indicates that the prediction of thermoelectric properties in a one-band model is valid as long as  $E_g/(2k_B T) \geq 10$ . Finally, we ask how electron Coulomb interactions influence the thermoelectric properties of a TL. If the wave functions of the electrons in each lattice are localized, the electron Coulomb interactions are strong. Their effects on electron transport are significant in the scenario of weak hopping strengths.[7] On the other hand, the wave functions of the electrons are delocalized in the scenario

of strong hopping strengths to form bands; hence their weak electron Coulomb interactions can be ignored. Our study belongs to the latter case.

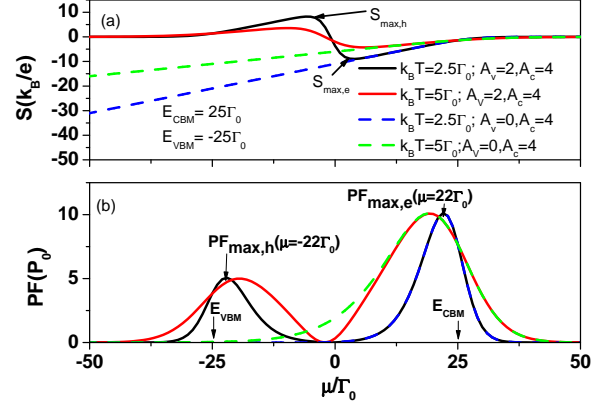


FIG. 7: (a) Seebeck coefficient  $S$  and (b) power factor  $PF$  as functions of  $\mu$  for two different temperatures at  $\Delta_c = -\Delta_v = 54 \Gamma_0$ ,  $E_{CBM} = 25 \Gamma_0$  and  $E_{VBM} = -25 \Gamma_0$ . Two curves considering one band model ( $A_v = 0$ ) are also plotted.

#### IV. CONCLUSION

We theoretically studied the thermoelectric properties of finite 2D TLs coupled to electrodes based on the framework of the tight-binding model, which does not need heavily numerical calculations like the first-principle methods. Electron-hole symmetry breaking appears in the power factor ( $PF$ ). This is attributed to the  $T_{LR}(\varepsilon)$  without the inversion symmetry of  $\varepsilon$ . In a negative  $S$  regime, a steep change in the transmission coefficient gives rise to a large electrical conductance. This explains why the maximum  $PF$  of electrons is larger than that of holes. According to Fig. 4, the contact between the electrodes and a 2D TL significantly influences the optimization of  $PF$ . In particular, the peak of  $PF$  for electrons at room temperature occurs at the position of chemical potential near the LBE of the 2D TLs. Besides, the enhancement of Ge with increasing electronic states will not suppress  $S$ . Such a remarkable thermoelectric property is very useful for achieving large  $PF$  values. Finally, we have demonstrated that the one-band model prediction is adequate when the band gap is ten times larger than  $k_B T$ .

#### Acknowledgments

We are grateful to Dr. Yia-Chung Chang for many encouraging conversations.

E-mail address: mtkuo@ee.ncu.edu.tw

- 
- <sup>1</sup> G. D. Mahan and J. O. Sofo, Proc. Natl. Acad. Sci. USA **93**, 7436 (1996).
  - <sup>2</sup> G. D. Mahan, L. M. Woods, Phys. Rev. Lett. **80**, 4016 (1998).
  - <sup>3</sup> G. Chen, Phys. Rev. B **57**, 14958 (1998).
  - <sup>4</sup> G. Chen, M. S. Dresselhaus, G. Dresselhaus, J. P. Fleurial, and T. Caillat, International Materials Reviews, **48**, 45 (2003).
  - <sup>5</sup> David. M.-T. Kuo and Y. C. Chang, Phys. Rev. B **81**, 205321 (2010).
  - <sup>6</sup> R. S. Whitney, Phys. Rev. Lett. **112**, 130601 (2014).
  - <sup>7</sup> David. M. T. Kuo, C. C. Chen and Y. C. Chang, Phys. Rev. B **95**, 075432 (2017).
  - <sup>8</sup> R. Venkatasubramanian, E. Siivola, T. Colpitts, B. OQuinn, Nature **413**, 597 (2001).
  - <sup>9</sup> A. I. Boukai, Y. Bunimovich, J. Tahir-Kheli, J. K. Yu, W. A. Goddard III and J. R. Heath, Nature, **451**, 168 (2008).
  - <sup>10</sup> T. C. Harman, P. J. Taylor, M. P. Walsh, B. E. LaForge, Science **297**, 2229 (2002).
  - <sup>11</sup> David. M. T. Kuo and Y. C. Chang, Nanotechnology, **24**, 175403 (2013).
  - <sup>12</sup> T. C. Kagan and C. B. Murry, Nat. Nanotechnology **10**, 1013 (2015).
  - <sup>13</sup> A. K. Geim, and I. V. Grigorieva, Nature **499**, 419 (2013).
  - <sup>14</sup> K. S. Novoselov, A. Mishchenko, A. Carvalho, and A. H. C. Neto, Science **353**, aac9439 (2016).
  - <sup>15</sup> S. B. Desai et al., Nano Lett. **14**, 4592 (2014).
  - <sup>16</sup> L. D. Zhao, S. H. Lo, Y. Zhang, H. Sun, G. Tan, C. Uher, C. Wolverton, V. P. Dravid and M. G. Kanatzidis, Nature **508**, 373 (2014).
  - <sup>17</sup> K. Hippalgaonkar, Y. Wang, Y. Ye, D. Y. Qiu, H. Zhu, Y. Wang, J. Moore, S. G. Louie and X. Zhang, Phys. Rev. B **95**, 115407 (2017).
  - <sup>18</sup> C. Chang, M. Mu, D. He, Y. Pei, and C. F. Wu et al., Science **360**, 778 (2018).
  - <sup>19</sup> D. D. Fan, H. J. Liu, L. Cheng, P. H. Jiang, J. Shi and X. F. Tang, Appl. Phys. Lett. **105**, 133113 (2014).
  - <sup>20</sup> W. Huang, X. Luo, C. K. Gan, S. Y. Quek and C. C. Liang, Phys. Chem. Chem. Phys. **16**, 10866 (2014).
  - <sup>21</sup> Y. L. Ouyang, Y. Xie, Z. W. Zhang, Q. Peng, and Y. P. Chen, J. Appl. Phys. **120**, 235109 (2016).
  - <sup>22</sup> G. Ozbal, R. T. Senger, C. Sevik and H. Sevineli, Phys. Rev. B **100**, 085415 (2019).
  - <sup>23</sup> H. Moon, J. Bang, S. Hong, G. Kim, J. W. Roh, J. Kim, and W. Lee, ACS Nano, **13**, 13317 (2019).
  - <sup>24</sup> Y. Wang et al, Nature **568**, 70 (2019).
  - <sup>25</sup> X. F. Qian, J. W. Liu, L. Fu, and J. Li, Science **346**, 1344 (2014).
  - <sup>26</sup> X. M. Wang et al, Nat. Nanotechnology **10**, 517 (2015).
  - <sup>27</sup> Y. Wang et al, Nature **550**, 487 (2017).
  - <sup>28</sup> A. Y. Lu et al, Nat. Nanotechnology **12**, 744 (2017).
  - <sup>29</sup> M. Y. Li et al, Science **349**, 524 (2015).
  - <sup>30</sup> A. D. Franklin, Science **349**, aab2750 (2015).
  - <sup>31</sup> D. Akinwande et al, Nature **573**, 507 (2019).
  - <sup>32</sup> J. Li et al, Nature **579**, 368 (2020).
  - <sup>33</sup> H. Haug and A. P. Jauho, Quantum Kinetics in Transport and Optics of Semiconductors (Springer, Heidelberg, 1996).
  - <sup>34</sup> D. M. T. Kuo, AIP Advances **10**, 045222 (2020).
  - <sup>35</sup> T. Horiguchi, Physica A **178**, 351 (1991).